PERTURBATIONS OF THE COUPLED JEFFERY-STOKES EQUATIONS

Abstract. This paper seeks to provide clues as to why experimental evidence for the alignment of fibers in semi-dilute suspensions under shear flows does not match theoretical predictions. This paper posits that it is the coupling between Jeffery's equation and Stokes' equation that causes the deviation from theory. It is proposed that if the initial data is slightly non-uniform, then there is feedback via Stokes' equation that causes these non-uniformities to grow significantly in short amounts of time, so that the standard uncoupled Jeffery's equation becomes a poor predictor. This paper provides numerical evidence, involving spectral analysis of the linearization of the perturbation equation, to support this theory.

1. Introduction

Jeffery's equation (Jeffery, 1923) has been used to predict the orientation of fibers in flows with low Reynolds number. Experiments performed for shear flows show that the prediction from Jeffery's equation is somewhat inaccurate. Firstly, the eventual steady state disagrees with the prediction from the Jeffery's equation. Secondly, Jeffery's equation for fibers with finite aspect ration ($|\lambda| < 1$) predicts that the fiber orientation is periodic in time, but this is not seen in experiments (see, for example, Anczurowski & Mason, 1967). Thirdly, the rate of alignment is much slower than predicted. The first and second points were successfully countered by adding diffusion terms to Jeffery's equation (Bird *et al.*, 1987), for example, the Folgar-Tucker equation (Folgar & Tucker, 1984). But experimental evidence shows that the diffusion terms fail to account for the delay in alignment, and the observed times for alignment are many times longer than the theoretically obtained values (see, for example, Nguyen *et al.*, 2008; Sepehr *et al.*, 2004; Wang *et al.*, 2008).

Jeffery's equation is a prediction of the evolution of the function ψ, the probability distribution of the orientation of fibers, at each point in time and space. This is a function $\psi(\mathbf{x}, \mathbf{p}, t)$ of the three variables space $\mathbf{x} \in \mathbb{R}^3$, time $t \geq 0$, and orientation $\mathbf{p} \in S$, where $S = \{\mathbf{p} = (p_1, p_2, p_3) : |\mathbf{p}|^2 = p_1^2 + p_2^2 + p_3^2 = 1\}$ is the two dimensional sphere. The equations involve the velocity field $\mathbf{u} = (u_1, u_2, u_3)$, which is a function of space $\mathbf{x}$ and time t. Associated with the velocity field $\mathbf{u}$ are the Jacobian matrix $\boldsymbol{\nabla}\mathbf{u} = (\partial u_i/\partial x_j)_{1\leq i,j\leq 3}$, the deformation matrix or rate of strain tensor $\Gamma = \boldsymbol{\nabla}\mathbf{u} + (\boldsymbol{\nabla}\mathbf{u})^T$, and the vorticity matrix $\Omega = \boldsymbol{\nabla}\mathbf{u} - (\boldsymbol{\nabla}\mathbf{u})^T$. Jeffery's equation is

$$\frac{\partial \psi}{\partial t} + \mathbf{u} \cdot \boldsymbol{\nabla}\psi = -\tfrac{1}{2}\boldsymbol{\nabla}_{\mathbf{p}} \cdot ((\Omega \cdot \mathbf{p} + \lambda(\Gamma \cdot \mathbf{p} - \Gamma : \mathbf{ppp}))\psi) \tag{1}$$

$$\psi = \tfrac{1}{4\pi} \text{ at } t = 0 \tag{2}$$

Here $\boldsymbol{\nabla}_{\mathbf{p}}$ denotes the gradient on the sphere S.

One possible cause for the lack of predictive power of Jeffery's equation might be that it fails to account for the fibers colliding with each other. Indeed, this is what the diffusion terms are meant to simulate. This paper gives a different possible

explanation of this delay in alignment. Our assertion is that if the initial state of ψ is not completely isotropic, then small perturbations grow, and after a short amount of time dramatically effect the solution. We do not produce a formula that predicts how the fibers orient, but we do cast doubt upon Jeffery's equation being able to produce a good prediction.

The orientation of fibers at each point effects the rheology of the fluid. A fiber that is oriented parallel or perpendicular to the principle axes of the rate of strain tensor is going to act like a 'stiffener' to the fluid, whereas a fiber that is oriented along a null direction of the rate of strain tensor (that is, if $\Gamma \cdot \mathbf{p} = 0$) does not hinder the flow in any way. It is posited in Lipscomb II *et al.* (1988) that if the underlying fluid is Newtonian, then the stress-strain relation is

$$\tau = \nu(\beta \mathbb{A} : \Gamma + \Gamma) \tag{3}$$

Here τ is the stress tensor, $\mathbb{A}$ is the 4th moment tensor

$$\mathbb{A} = \int_S \mathbf{pppp}\, \psi \, d\mathbf{p} \tag{4}$$

ν is the underlying Newtonian viscosity of the fluid (which we may as well set to unity), and β is a dimensionless quantity that is related to the volume fraction of the fibers in the fluid. The quantity β represents the extent to which fibers act as 'stiffeners' to the fluid motion. We refer to the case $\beta = 0$ as the uncoupled Jeffery's equation. The paper Sepehr *et al.* (2004) suggests that $\beta = 50$ might be a reasonable value.

We assume that Reynolds number is close to zero, and so we neglect inertial terms. We also assume the fluid is incompressible. Then the velocity field obeys the following Stokes' equation, where p denotes pressure.

$$\boldsymbol{\nabla} \cdot (\tau - pI) = 0 \tag{5}$$

$$\boldsymbol{\nabla} \cdot \mathbf{u} = 0 \tag{6}$$

To simplify the mathematics, we assume that the fluid occupies the whole of three dimensional space, and that there is an 'ambient' velocity gradient U, a three by three matrix with trace zero, so that

$$\boldsymbol{\nabla} \mathbf{u} \to U \text{ as } \mathbf{x} \to \infty \tag{7}$$

If ψ does not initially depend upon $\mathbf{x}$, then it can be rather quickly seen that a solution is $\mathbf{u} = U \cdot \mathbf{x}$ for all $t \geq 0$. This is also a solution when $\beta = 0$, even when ψ does depend upon $\mathbf{x}$.

We propose that large changes in fiber orientation are created by initially small perturbations in the fiber orientation, which in a short amount of time are greatly enlarged. An example of this is a kind of 'buckling' effect, that we illustrate in Figure 1. This illustrates an elongation flow where the fluid is squeezed along the y axis, is expanded along the x axis, and no elongation takes place along the z axis, that is, $\boldsymbol{\nabla}\mathbf{u} = \left[\begin{smallmatrix} G & 0 & 0 \\ 0 & -G & 0 \\ 0 & 0 & 0 \end{smallmatrix}\right]$ for some $G > 0$. The small ellipsoids represent the orientation of a small proportion of the fibers that represent the majority of orientations of the perturbation, and show a small perturbation of ψ of the form $\epsilon\hat{\psi}\sin(2\pi y/L)$. It is reasonable to expect that this perturbation causes the fibers to 'buckle,' that is, create perturbations to $\mathbf{u}$ of the form $\epsilon \left[\begin{smallmatrix} 0 \\ 0 \\ \hat{u}_3 \end{smallmatrix}\right] \cos(2\pi y/L)$. This then

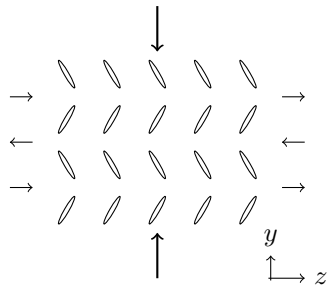

FIGURE 1. 'Buckling' caused by elongation flow applied to a non-constant fiber orientation distribution.

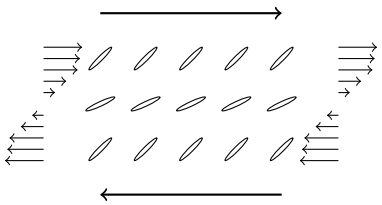

FIGURE 2. Shear-banding caused by shear flow applied to a non-constant fiber orientation distribution.

feeds back into the perturbation of ψ causing it to grow exponentially. (We later demonstrate that this buckling can take place in any direction in the yz-plane.)

Another possibility is a self-reinforcing shear-banding that is illustrated in Figure 2 (although it can only happen as a perturbation of a flow that is no longer isotropic).

Thus if the fibers are not initially oriented homogeneous with respect to space, then over a reasonably short span of time, regions of low and high viscosity are created. The regions of high viscosity will tend to group together and move as a bulk. One possible scenario is shown in Figure 3 for a shear flow, but we emphasize that we have no reason to suppose this situation over any other complex situation (particularly as in this picture we do not show viscosity as anisotropic). Many similar scenarios could conceivably slow down the rate of alignment of the fibers. In the conclusion, we suggest that this variation in viscosity takes place at small length scales, and so is hard to see experimentally.

To summarize, in this paper we simply seek to show that small perturbations become larger in a short amount of time. We examine the linearized equation for the perturbation. We propose that when the perturbations become large, that the linear approximation becomes inaccurate, and that the solution becomes hard to predict, and is likely to deviate greatly from the solution to the unperturbed Jeffery's equation. In this paper, we give some evidence to the former assertion, but leave the latter assertion to later works. We discuss the extent to which we have been successful in this endeavor in the conclusion.

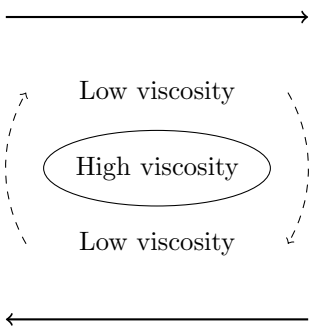

FIGURE 3. A fluid of varying viscosity reacting to a shear flow.

2. A heuristic demonstration of 'buckling'

Before embarking on the detailed arguments, let us start by giving a simple, albeit imprecise, argument for the 'bucking' shown in Figure 1. If the fiber distribution is isotropic, that is, $\psi = 1/4\pi$, then it can be shown that the 4th moment tensor is given by $\mathbb{A}_{iiii} = \frac{1}{5}$, $\mathbb{A}_{iijj} = \frac{1}{15}$, $\mathbb{A}_{ijkk} = 0$ (here $i \neq j \neq k$). Now, following Figure 1, let us suppose that there are an additional small proportion of fibers in the direction $\mathbf{p}_1 = \frac{1}{\sqrt{2}}(0,1,1)$ with proportion $\epsilon \sin(2\pi y/L)$, and an additional small proportion of fibers in the direction $\mathbf{p}_2 = \frac{1}{\sqrt{2}}(0,1,-1)$ with proportion $-\epsilon \sin(2\pi y/L)$. Here ϵ is small. Thus we perturb $\mathbb{A}$ by making the replacement

$$\mathbb{A} \to \mathbb{A} + \epsilon \sin(2\pi y/L)\tilde{\mathbb{A}} \tag{8}$$

where

$$\tilde{\mathbb{A}} = (\mathbf{p}_1\mathbf{p}_1\mathbf{p}_1\mathbf{p}_1 - \mathbf{p}_2\mathbf{p}_2\mathbf{p}_2\mathbf{p}_2) \tag{9}$$

that is, $\tilde{\mathbb{A}}_{ijkl} = 1/2$ whenever (i,j,k,l) is a permutation of $(2,2,2,3)$ or $(2,3,3,3)$, and all other entries of $\mathbb{A}$ are zero. Looking for solutions to equations (3), (5), and (6) of the form

$$\mathbf{u} = \begin{bmatrix} Gx \\ -Gy \\ 0 \end{bmatrix} + \epsilon \sin(2\pi y/L) \begin{bmatrix} \hat{u}_1 \\ \hat{u}_2 \\ \hat{u}_3 \end{bmatrix} + \epsilon \cos(2\pi y/L) \begin{bmatrix} \hat{v}_1 \\ \hat{v}_2 \\ \hat{v}_3 \end{bmatrix} \tag{10}$$

$$p = \epsilon \sin(2\pi y/L)\hat{p}_1 + \epsilon \cos(2\pi y/L)\hat{p}_2 \tag{11}$$

we obtain $\hat{u}_1 = \hat{u}_2 = \hat{u}_3 = \hat{v}_1 = \hat{v}_2 = \hat{p}_1 = \hat{p}_2 = 0$ and $\hat{v}_3 = -\frac{15GL\beta}{2\pi(15+2\beta)} < 0$. This is a velocity field behaving exactly as shown in Figure 1, and it is clear that this will cause more fibers to move towards the $\mathbf{p}_1$ direction when $\sin(2\pi y/L) > 0$, and more fibers to move towards the $\mathbf{p}_2$ direction when $\sin(2\pi y/L) < 0$.

This argument should be regarded as merely heuristic, in part because the underlying probability distribution ψ in our description is not non-negative on all of S.

3. The nature of the perturbations

We perturb ψ by applying the replacement

$$\psi \to \psi + \epsilon\tilde{\psi} \tag{12}$$

assuming that both ψ and its perturbation satisfy equations (1), (3), (5), (4) and (7). (Note that ψ, but not its perturbation, satisfies equation (2). Hence ψ, but not its perturbation, does not depend upon $\mathbf{x}$.) The idea is that if ϵ is small, then one assumes that terms of order ϵ^2 and higher can be ignored, and from the terms of order ϵ we form a differential equation in $\tilde{\psi}$. Furthermore, this differential equation is linear in $\tilde{\psi}$, although the coefficients of the differential equation depend upon ψ in possibly a highly non-linear manner. The thinking is that if the linearized perturbations $\tilde{\psi}$ grow by a large amount, that one might expect the terms of order ϵ^2 and higher to have a large effect on the solution, and that the linearization is no longer valid.

At least for ordinary differential equations, there is already a well established theory (see, for example, Chicone, 2006; Strogatz, 1994) on how to analyze these perturbations in the case that the unperturbed ψ satisfies the steady-state form of the equation, and if one is interested in instabilities that occur asymptotically as $t \to \infty$. One analyzes the eigenvalues of the linear differential operator of $\tilde{\psi}$, and if any of the eigenvalues have positive real part, then the perturbations grow, and the differential equation for ψ is unstable around this steady state.

Another well established theory, the theory of Floquet multipliers, can be applied when the unperturbed equation has a periodic solution. This is what happens in a shear flow when $|\lambda| < 1$, when in theory, the fibers 'tumble' in so called Jeffery's orbits. We will examine the Floquet multipliers, and see strong evidence that the solutions are linearly unstable. This, we suggest, explains why the Jeffery's tumbling does not seem to be observed in experiments for shear flows of semi-dilute suspensions (see Anczurowski & Mason, 1967).

However the situation upon which we wish to focus most attention is for shear flow with slender fibers $\lambda = 1$. Then ψ does not satisfy a steady state equation, nor is it periodic, nor are we interested in asymptotic behavior. For this reason, we provide heuristic rather than definitive arguments, which we now explain. What we are interested in are perturbations that cause a large change in behavior. It is instructive to consider the same perturbation when evolved by the uncoupled Jeffery-Stokes system, that is, when $\beta = 0$. In this case, the fiber orientation does not effect the velocity field, and a solution is $\mathbf{u} = U \cdot \mathbf{x}$ for all time. But perturbations are still quite likely to grow exponentially, by virtue of being carried by the shear flow, and this simply reflects growth caused by the unperturbed ψ. We refer to these perturbations as 'uninteresting.' What we are looking for are 'interesting' perturbations, which when allowed to grow large enough cause the kind of behavior illustrated in Figure 3.

The way we propose to do this is to solve the coupled equation for the perturbed ψ, and then take this as the initial value and solve for ψ at $t = 0$ by evolving the equation with $\beta = 0$ backwards in time. Fortunately Jeffery's equation has no diffusion type terms, and is completely time reversible. For now, we take it on faith that this might be a good approach, but in equation (35) we provide some partial justification, at least for this specific equation, why we think this gives a good indication of the kinds of perturbations that greatly influence the full solution.

Next, we can write the perturbation as a Fourier transform

$$\tilde{\psi}(\mathbf{x}, \mathbf{p}, t) = \iiint \hat{\psi}(\boldsymbol{\kappa}, \mathbf{p}, t) e^{i\boldsymbol{\kappa}\cdot\mathbf{x}} \, d\boldsymbol{\kappa} \tag{13}$$

It can be seen that if we consider only terms of order ϵ and lower, the different terms of the integrand do not interact. As long as one assumes that $\boldsymbol{\kappa}$ evolves according to equation (16) (see below), without loss of generality, we can assume that the perturbation is of the form

$$\psi \to \psi + \epsilon\hat{\psi}e^{i\boldsymbol{\kappa}\cdot\mathbf{x}} \tag{14}$$

for some wave number $\boldsymbol{\kappa}$. While this solution involves complex numbers, by considering linear combinations, we see that $e^{i\boldsymbol{\kappa}\cdot\mathbf{x}}$ is simply 'code' for $\sin(\boldsymbol{\kappa}\cdot\mathbf{x})$, and similarly $ie^{i\boldsymbol{\kappa}\cdot\mathbf{x}}$ is the same solution that is 90° out of phase, that is, $\cos(\boldsymbol{\kappa}\cdot\mathbf{x})$. Note that this kind of perturbed quantity does not allow the boundary condition (7) for $\mathbf{u}$, but this is not a real problem, since we know that ultimately these terms come from equation (13), and that $\tilde{\psi}$ does satisfy this boundary condition.

In order to satisfy Jeffery's equation, we require that $\boldsymbol{\kappa}$ satisfy

$$\left(\frac{\partial}{\partial t} + \mathbf{u}\cdot\boldsymbol{\nabla}\right)(\hat{\psi}e^{i\boldsymbol{\kappa}\cdot\mathbf{x}}) = \frac{\partial\hat{\psi}}{\partial t}\,e^{i\boldsymbol{\kappa}\cdot\mathbf{x}} + O(\epsilon) \tag{15}$$

To make this happen, we evolve $\boldsymbol{\kappa}$ according to the equation

$$\frac{\partial}{\partial t}\boldsymbol{\kappa} = -U^T\cdot\boldsymbol{\kappa} \tag{16}$$

$$\boldsymbol{\kappa} = \boldsymbol{\kappa}_0 \text{ at } t = 0 \tag{17}$$

Equation (15) then follows because

$$\frac{\partial}{\partial t}e^{i\boldsymbol{\kappa}\cdot\mathbf{x}} = -i[(U^T\cdot\boldsymbol{\kappa})\cdot\mathbf{x}]e^{i\boldsymbol{\kappa}\cdot\mathbf{x}} = -(U\cdot\mathbf{x})\cdot(i\boldsymbol{\kappa})e^{i\boldsymbol{\kappa}\cdot\mathbf{x}} = -\mathbf{u}\cdot\boldsymbol{\nabla}[e^{i\boldsymbol{\kappa}\cdot\mathbf{x}}] + O(\epsilon) \tag{18}$$

Note that if U does not depend upon t, then equations (16) and (17) are solved by

$$\boldsymbol{\kappa} = e^{-tU^T}\boldsymbol{\kappa}_0 \tag{19}$$

4. Solution of the unperturbed Jeffery's equation

By Lipscomb II *et al.* (1988); Dinh & Armstrong (1984); Szeri & Lin (1996), it is known that the solution to equation (1) and (2) is

$$\psi(\mathbf{p}) = \frac{1}{4\pi(B:\mathbf{pp})^{3/2}} \tag{20}$$

where the matrix B satisfies

$$\frac{\partial B}{\partial t} + \mathbf{u}\cdot\boldsymbol{\nabla}B = -\tfrac{1}{2}B\cdot(\Omega+\lambda\Gamma) - \tfrac{1}{2}(-\Omega+\lambda\Gamma)\cdot B \tag{21}$$

$$B = I \text{ at } t = 0 \tag{22}$$

or equivalently

$$B = C^T\cdot C \tag{23}$$

where C satisfies the equation

$$\frac{\partial C}{\partial t} + \mathbf{u}\cdot\boldsymbol{\nabla}C = -\tfrac{1}{2}C\cdot(\Omega+\lambda\Gamma) \tag{24}$$

$$C = I \text{ at } t = 0 \tag{25}$$

The 4th order moment tensor $\mathbb{A}$ can be calculated directly from B using elliptic integrals Montgomery-Smith *et al.* (2010*a*) (see also Verleye & Dupret, 1993; VerWeyst, 1998)

$$\mathbb{A} = \mathbb{A}(B) = \tfrac{3}{4}\int_0^\infty \frac{s\,\mathcal{S}((B+sI)^{-1}\otimes(B+sI)^{-1})\,ds}{\sqrt{\det(B+sI)}} \tag{26}$$

where $\mathcal{S}$ is the symmetrization of a tensor, that is, if $\mathbb{B}$ is a rank n tensor, then $\mathcal{S}(\mathbb{B})_{i_1\dots i_n}$ is the average of $\mathbb{B}_{j_1\dots j_n}$ over all permutations $(j_1,\dots,j_n)$ of $(i_1,\dots,i_n)$.

It can be seen from equations (1) and (2) that since ψ starts out taking values independent of $\mathbf{x}$, then ψ stays independent of $\mathbf{x}$. In particular, the terms $\mathbf{u}\cdot\boldsymbol{\nabla}\psi$ and $\mathbf{u}\cdot\boldsymbol{\nabla}C$ are zero. Also,

$$\Gamma = U + U^T \tag{27}$$

$$\Omega = U - U^T \tag{28}$$

The equation for ψ or C is now decoupled from the equation for $\mathbf{u}$. In particular, if U is independent of t, it can be easily computed by

$$C = \exp\left(-\tfrac{1}{2}t(\Omega+\lambda\Gamma)\right) \tag{29}$$

5. The Linearized Equations

At time $t=0$, we introduce a small, linear perturbation that oscillates in space with wave number $\boldsymbol{\kappa}$, that is, we perform the replacement

$$B \to B + \epsilon\hat{B}e^{i\boldsymbol{\kappa}\cdot\mathbf{x}} \tag{30}$$

Here we suppose that ϵ is small, and the process of linearization is to neglect terms in ϵ of orders two and higher.

As we described above, our approach is to measure this perturbed B by pulling it backwards in time to $t=0$ using the Jeffery-Stokes equation with $\beta=0$. Let us refer by $\bar{B}$ the backwards in time solution of equation (21) with $\beta=0$. Thus we are going to find $\bar{B}(0)$ when

$$\frac{\partial\bar{B}}{\partial t} + \mathbf{u}\cdot\boldsymbol{\nabla}\bar{B} = -\tfrac{1}{2}\bar{B}\cdot(\Omega+\lambda\Gamma)) - \tfrac{1}{2}(-\Omega+\lambda\Gamma))\cdot\bar{B} \tag{31}$$

$$\bar{B} = B + \epsilon\hat{B}e^{i\boldsymbol{\kappa}\cdot\mathbf{x}} \text{ at time } t \tag{32}$$

and this is solved by

$$\bar{B}(0) = I + \epsilon(C^T)^{-1}\cdot\hat{B}\cdot C^{-1}\,e^{i\boldsymbol{\kappa}_0\cdot\mathbf{x}} \tag{33}$$

(see equation (15) for why the $\mathbf{u}\cdot\boldsymbol{\nabla}$ gives rise to the $\boldsymbol{\kappa}_0$ in the exponential).

This tells us that the quantity we measure is

$$\tilde{B} = (C^T)^{-1}\cdot\hat{B}\cdot C^{-1} \tag{34}$$

Note that $\tilde{B}$ is symmetric, and because we need to preserve $\det(B)=1$, we have the relation $\mathrm{Tr}(\tilde{B})=0$. Also, we have

$$B + \epsilon\hat{B}e^{i\boldsymbol{\kappa}\cdot\mathbf{x}} = C^T\cdot(I+\epsilon\tilde{B}\,e^{i\boldsymbol{\kappa}\cdot\mathbf{x}})\cdot C \tag{35}$$

This means that we can easily quantify how the size of $\epsilon\tilde{B}$ really effects the fiber orientation, namely that B is significantly effected if the spectral radius of $\epsilon\tilde{B}$ (which is equal to its spectral norm) is large. This provides additional evidence to support the notion that $\tilde{B}$ is the right quantity to measure.

The goal is to create an equation

$$\frac{\partial \tilde{B}}{\partial t} = M(\boldsymbol{\kappa}, t)[\tilde{B}] \tag{36}$$

where $M(\boldsymbol{\kappa}, t)$ is linear operator acting upon symmetric, trace zero matrices, depending (amongst other things) upon $\boldsymbol{\kappa}$.

We make the additional replacements

$$\mathbf{u} \to U \cdot \mathbf{x} + \epsilon \hat{\mathbf{u}} e^{i\boldsymbol{\kappa}\cdot\mathbf{x}} \tag{37}$$

$$\Gamma \to \Gamma + \epsilon \hat{\Gamma} e^{i\boldsymbol{\kappa}\cdot\mathbf{x}} \tag{38}$$

$$\Omega \to \Omega + \epsilon \hat{\Omega} e^{i\boldsymbol{\kappa}\cdot\mathbf{x}} \tag{39}$$

$$\tau \to \tau + \epsilon \hat{\tau} e^{i\boldsymbol{\kappa}\cdot\mathbf{x}} \tag{40}$$

$$p \to p + \epsilon \hat{p} e^{i\boldsymbol{\kappa}\cdot\mathbf{x}} \tag{41}$$

$$\mathbb{A} \to \mathbb{A} + \epsilon \hat{\mathbb{A}} e^{i\boldsymbol{\kappa}\cdot\mathbf{x}} \tag{42}$$

The linearized equations can be shown to be

$$\frac{\partial \tilde{B}}{\partial t} = -\tfrac{1}{2} C \cdot (\hat{\Omega} + \lambda \hat{\Gamma}) \cdot C^{-1} - \tfrac{1}{2} (C^T)^{-1} \cdot (-\hat{\Omega} + \lambda \hat{\Gamma}) \cdot C^T \tag{43}$$

$$\hat{\mathbb{A}} = \frac{\partial \mathbb{A}}{\partial B} : (C^T \cdot \tilde{B} \cdot C) \tag{44}$$

$$\hat{\Gamma} = i(\boldsymbol{\kappa}\hat{\mathbf{u}} + \hat{\mathbf{u}}\boldsymbol{\kappa}) \tag{45}$$

$$\hat{\Omega} = i(\boldsymbol{\kappa}\hat{\mathbf{u}} - \hat{\mathbf{u}}\boldsymbol{\kappa}) \tag{46}$$

$$\hat{\tau} = \beta \mathbb{A} : \hat{\Gamma} + \beta \hat{\mathbb{A}} : \Gamma + \hat{\Gamma} \tag{47}$$

$$\boldsymbol{\kappa} \cdot (\hat{\tau} - \hat{p} I) = 0 \tag{48}$$

$$\boldsymbol{\kappa} \cdot \hat{\mathbf{u}} = 0 \tag{49}$$

$$\frac{\partial \mathbb{A}}{\partial B} = -\tfrac{15}{8} \int_0^\infty \frac{s\, \mathcal{S}[(B+sI)^{-1} \otimes (B+sI)^{-1} \otimes (B+sI)^{-1}]\, ds}{\sqrt{\det(B+sI)}} \tag{50}$$

noting here that $\frac{\partial \mathbb{A}}{\partial B}$ is a rank 6 tensor.

Let us provide some details of the derivation of equation (43). Substituting equations (30), (38) and (39) into equation (21), and retaining only the terms of order ϵ, we obtain

$$\begin{aligned} \frac{\partial}{\partial t}(\hat{B}\, e^{i\boldsymbol{\kappa}\cdot\mathbf{x}}) + \mathbf{u} \cdot \boldsymbol{\nabla}(\hat{B}\, e^{i\boldsymbol{\kappa}\cdot\mathbf{x}}) = &-\tfrac{1}{2}\hat{B} \cdot (\Omega + \lambda\Gamma)\, e^{i\boldsymbol{\kappa}\cdot\mathbf{x}} - \tfrac{1}{2}(-\Omega + \lambda\Gamma) \cdot \hat{B}\, e^{i\boldsymbol{\kappa}\cdot\mathbf{x}} \\ &- \tfrac{1}{2} B \cdot (\hat{\Omega} + \lambda\hat{\Gamma})\, e^{i\boldsymbol{\kappa}\cdot\mathbf{x}} - \tfrac{1}{2}(-\hat{\Omega} + \lambda\hat{\Gamma}) \cdot B\, e^{i\boldsymbol{\kappa}\cdot\mathbf{x}} \end{aligned} \tag{51}$$

Applying equations (15), (24) and (34), dividing by $e^{i\boldsymbol{\kappa}\cdot\mathbf{x}}$, and neglecting terms of order ϵ and higher, we obtain

$$C^T \cdot \frac{\partial \tilde{B}}{\partial t} \cdot C = -\tfrac{1}{2} B \cdot (\hat{\Omega} + \lambda\hat{\Gamma}) - \tfrac{1}{2}(-\hat{\Omega} + \lambda\hat{\Gamma}) \cdot B \tag{52}$$

and equation (43) is established.

Next, setting

$$N = |\boldsymbol{\kappa}|^2 I + 2\beta \mathbb{A} : \boldsymbol{\kappa}\boldsymbol{\kappa} \tag{53}$$

we have that equations (47), (48) and (49) can be replaced by

$$\hat{\mathbf{u}} = i\beta \left(I - \frac{N^{-1} \cdot \boldsymbol{\kappa}\boldsymbol{\kappa}}{N^{-1} : \boldsymbol{\kappa}\boldsymbol{\kappa}} \right) \cdot N^{-1} \cdot (\hat{\mathbb{A}} : \Gamma) \cdot \boldsymbol{\kappa} \tag{54}$$

To see this, note first that N is positive definite, and hence invertible. Substitute equations (45) and (47) into (48), and apply equation (49), to obtain

$$\hat{\mathbf{u}} + N^{-1} \cdot \boldsymbol{\kappa}\hat{p} = i\beta N^{-1} \cdot (\hat{\mathbb{A}} : \Gamma) \cdot \boldsymbol{\kappa} \tag{55}$$

Dot producting both sides with $\boldsymbol{\kappa}$, and again applying equation (49), yields

$$\hat{p} = i\beta \frac{\boldsymbol{\kappa} \cdot N^{-1} \cdot (\hat{\mathbb{A}} : \Gamma) \cdot \boldsymbol{\kappa}}{N^{-1} : \boldsymbol{\kappa}\boldsymbol{\kappa}} \tag{56}$$

Substituting this into equation (55) gives equation (54).

Finally, it is important to note that in equation (36), that $M(\boldsymbol{\kappa}, t)$ only depends on the direction of $\boldsymbol{\kappa}$, not on its length.

6. Linear perturbations of the fourth moment tensor

Equation (50) follows, since by differentiating equation (26) we have for any symmetric matrix $\hat{B}$

$$\begin{aligned} \frac{\partial \mathbb{A}}{\partial B} : \hat{B} &= \frac{d}{dt} \left[\mathbb{A}(B + t\hat{B}) \right] \Big|_{t=0} \\ &= -\tfrac{3}{2} \int_0^\infty \frac{s\, \mathcal{S}[((B+sI)^{-1} \cdot \hat{B} \cdot (B+sI)^{-1}) \otimes (B+sI)^{-1}]\, ds}{\sqrt{\det(B+sI)}} \\ &\quad -\tfrac{3}{8} \int_0^\infty \frac{s\, \mathrm{Tr}[(B+sI)^{-1} \cdot \hat{B}]\, \mathcal{S}[(B+sI)^{-1} \otimes (B+sI)^{-1}]\, ds}{\sqrt{\det(B+sI)}} \end{aligned} \tag{57}$$

and noting that for any symmetric matrix K

$$\mathcal{S}(K \otimes K \otimes K) : \hat{B} = \tfrac{4}{5} \mathcal{S}((K \cdot \hat{B} \cdot K) \otimes K) + \tfrac{1}{5} \mathrm{Tr}(K \cdot \hat{B})\, \mathcal{S}(K \otimes K) \tag{58}$$

To compute $\frac{\partial \mathbb{A}}{\partial B}$ in practice, one first diagonalizes B using an orthogonal similarity matrix, so that $B = \mathrm{diagonal}(b_1, b_2, b_3)$. In this case, the following kinds of quantities appear

$$\mathcal{E}^n_{m_1,m_2,m_3} = \int_0^\infty \frac{s^n\, ds}{(b_1+s)^{m_1+\frac{1}{2}} (b_2+s)^{m_2+\frac{1}{2}} (b_3+s)^{m_3+\frac{1}{2}}} \tag{59}$$

where m_1, m_2, m_3 and n are non-negative integers satisfying $n \leq m_1 + m_2 + m_3$. For example, it is shown in Montgomery-Smith *et al.* (2010*a*) that the 4th moment tensor is given by the formulae (here $i \neq j \neq k$)

$$\mathbb{A}_{iiii} = \tfrac{3}{4} \mathcal{E}^1_{2\delta_{i1}, 2\delta_{i2}, 2\delta_{i3}} \tag{60}$$

$$\mathbb{A}_{iijj} = \tfrac{1}{4} \mathcal{E}^1_{\delta_{i1}+\delta_{j1}, \delta_{i2}+\delta_{j2}, \delta_{i3}+\delta_{j3}} \tag{61}$$

$$\mathbb{A}_{ijkk} = 0 \tag{62}$$

where δ_{ij} denotes the Kronecker delta symbol. To compute $\mathcal{E}^n_{m_1,m_2,m_3}$, they are Carlson forms of elliptic integrals (Carlson, 1995) if $n = 0$ and $m_1 + m_2 + m_3 = 0$ or 1. Furthermore, if b_1, b_2 and b_3 are distinct, then the other quantities can be

calculated using the following types of relations (the only mildly difficult equality is the first, which requires a single application of integration by parts):

(63)
$$(m_1+\tfrac{1}{2})\mathcal{E}^{n+1}_{m_1+1,m_2,m_3}+(m_2+\tfrac{1}{2})\mathcal{E}^{n+1}_{m_1,m_2+1,m_3}+(m_3+\tfrac{1}{2})\mathcal{E}^{n+1}_{m_1,m_2,m_3+1}=(n+1)\mathcal{E}^{n}_{m_1,m_2,m_3}$$

$$\mathcal{E}^{n}_{m_1,m_2+1,m_3+1}=(b_2-b_3)^{-1}(\mathcal{E}^{n}_{m_1,m_2,m_3+1}-\mathcal{E}^{n}_{m_1,m_2+1,m_3}) \tag{64}$$

$$\mathcal{E}^{n}_{m_1+1,m_2,m_3+1}=(b_3-b_1)^{-1}(\mathcal{E}^{n}_{m_1+1,m_2,m_3}-\mathcal{E}^{n}_{m_1,m_2,m_3+1}) \tag{65}$$

$$\mathcal{E}^{n}_{m_1+1,m_2+1,m_3}=(b_1-b_2)^{-1}(\mathcal{E}^{n}_{m_1,m_2+1,m_3}-\mathcal{E}^{n}_{m_1+1,m_2,m_3}) \tag{66}$$

$$\mathcal{E}^{n+1}_{m_1+1,m_2,m_3}=\mathcal{E}^{n}_{m_1,m_2,m_3}-b_1\mathcal{E}^{n}_{m_1+1,m_2,m_3} \tag{67}$$

$$\mathcal{E}^{n+1}_{m_1,m_2+1,m_3}=\mathcal{E}^{n}_{m_1,m_2,m_3}-b_2\mathcal{E}^{n}_{m_1,m_2+1,m_3} \tag{68}$$

$$\mathcal{E}^{n+1}_{m_1,m_2,m_3+1}=\mathcal{E}^{n}_{m_1,m_2,m_3}-b_3\mathcal{E}^{n}_{m_1,m_2,m_3+1} \tag{69}$$

From a numerical perspective, good approximations to these elliptic integrals can also be found when the eigenvalues are not distinct by artificially adding a small term to some of the eigenvalues to make them distinct. To avoid excessive floating point errors, the eigenvalues need to be quite far from each other, for example, using IEEE double precision arithmetic we found that the eigenvalues have to be at least 10^{-6} from each other to get reasonable results when $m_1+m_2+m_3\leq 3$.

If $i\neq j\neq k\neq i$, we have the formulae

$$\left(\frac{\partial\mathbb{A}}{\partial B}\right)_{iiiiii}=-\tfrac{15}{8}\mathcal{E}^1_{3\delta_{i1},3\delta_{i2},3\delta_{i3}} \tag{70}$$

$$\left(\frac{\partial\mathbb{A}}{\partial B}\right)_{iiiijj}=-\tfrac{3}{8}\mathcal{E}^1_{2\delta_{i1}+\delta_{j1},2\delta_{i2}+\delta_{j1},2\delta_{i3}+\delta_{j1}} \tag{71}$$

$$\left(\frac{\partial\mathbb{A}}{\partial B}\right)_{iijjkk}=-\tfrac{1}{8}\mathcal{E}^1_{\delta_{i1}+\delta_{j1}+\delta_{k1},\delta_{i2}+\delta_{j2}+\delta_{k2},\delta_{i3}+\delta_{j3}+\delta_{k3}} \tag{72}$$

and all terms which have any index appearing precisely an odd number of times are 0.

If the eigenvalues are all the same, that is, $B=I$, then equation (50) simplifies to the formula

$$\frac{\partial\mathbb{A}}{\partial B}=-\tfrac{3}{14}\mathcal{S}(I\otimes I\otimes I) \tag{73}$$

7. Demonstration of 'buckling'

The linear operator $M(\boldsymbol{\kappa},0)$ in equation (36) can be computed using equations (23), (24), (25), (26), (27), (28), (43), (44), (45), (46), (54) and (73).

The idea is to compute the eigenvalues of the linear operator $M(\boldsymbol{\kappa},0)$ for various values of $\boldsymbol{\kappa}$, and to see if any of them have positive real part. Having computed the eigenvalues of $M(\boldsymbol{\kappa},0)$, we feed them into equation (54) to see if they produce a significant perturbation to $\mathbf{u}$, and to see in what direction these perturbations take place.

The operator $M(\boldsymbol{\kappa},t)$ acts on the space of symmetric, trace zero, 3×3 matrices. This is a five dimensional space, and with respect to the Frobenius norm, has an

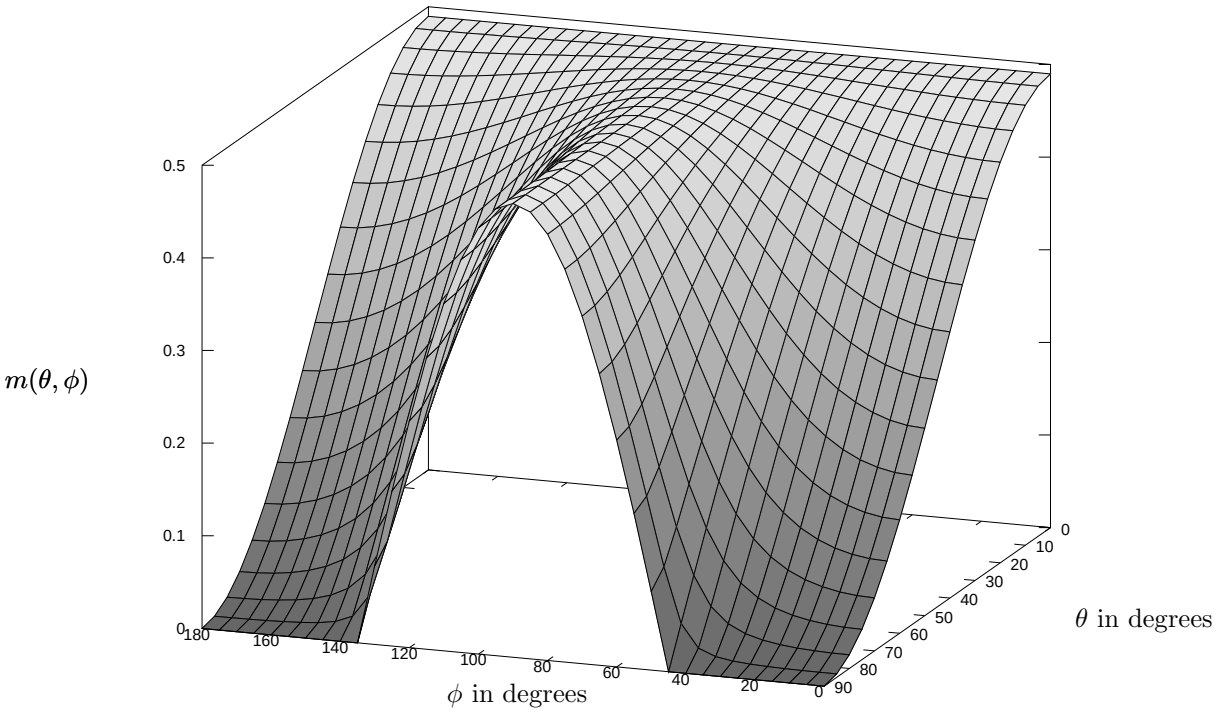

FIGURE 4. Graph of largest real part of eigenvalue of $\mathcal{M}(\boldsymbol{\kappa}, 0)$ under elongation flow.

orthogonal basis

$$T_1 = \frac{1}{\sqrt{2}}\begin{bmatrix} 1 & 0 & 0 \\ 0 & -1 & 0 \\ 0 & 0 & 0 \end{bmatrix}, \quad T_2 = \frac{1}{\sqrt{2}}\begin{bmatrix} 0 & 1 & 0 \\ 1 & 0 & 0 \\ 0 & 0 & 0 \end{bmatrix}, \quad T_3 = \frac{1}{\sqrt{6}}\begin{bmatrix} 1 & 0 & 0 \\ 0 & 1 & 0 \\ 0 & 0 & -2 \end{bmatrix}, \tag{74}$$
$$T_4 = \frac{1}{\sqrt{2}}\begin{bmatrix} 0 & 0 & 1 \\ 0 & 0 & 0 \\ 1 & 0 & 0 \end{bmatrix}, \quad T_5 = \frac{1}{\sqrt{2}}\begin{bmatrix} 0 & 0 & 0 \\ 0 & 0 & 1 \\ 0 & 1 & 0 \end{bmatrix}$$

Thus in order to examine the eigenvalues of $M(\boldsymbol{\kappa}, t)$, it is equivalent to compute the eigenvalues of $\mathcal{M}(\boldsymbol{\kappa}, t)$ where

$$\mathcal{M}(\boldsymbol{\kappa}, t)_{i,j} = \mathrm{Tr}(T_i \cdot (M(\boldsymbol{\kappa}, t)[T_j])) \tag{75}$$

In Figure 4 we display $m(\theta, \phi)$, the largest real part of the eigenvalues of $\mathcal{M}(\boldsymbol{\kappa}, 0)$, with elongation flow $\boldsymbol{\nabla}\mathbf{u} = \begin{bmatrix} 1 & 0 & 0 \\ 0 & -1 & 0 \\ 0 & 0 & 0 \end{bmatrix}$ and $\lambda = 1$ and $\beta = 10$. This was computed using the software product *Mathematica* by Wolfram Research, Inc., and independently verified by the software described in the next section. We only need to consider $\boldsymbol{\kappa}$ on the unit sphere, that is, when $\boldsymbol{\kappa} = (\cos(\phi)\sin(\theta), \sin(\phi)\sin(\theta), \cos(\theta))$, with $0 < \phi < \pi$ and $0 < \theta < \pi/2$.

We see that this becomes particularly large, with value $24/49$, when $\phi = 90°$. For example, if $(\theta, \phi) = (90°, 90°)$, then equation (54) gives $\hat{\mathbf{u}} = (0, 0, 24/49)$. This is exactly the kind of buckling illustrated in Figure 1. When $\theta = 0$, we find that $\hat{\mathbf{u}} = \pm(0, 24/49, 0)$, that is, the fibers slide past each other in the xy-plane in a direction parallel to the y-axis.

Notice that the perturbations use all three dimensions. Simulations of the coupled system have usually been performed in only two dimensions (Chinesta & Poitou, 2002; Chinesta *et al.*, 2003), or at least with some assumption of symmetry that effectively limits the spacial degrees of freedom to two dimensions (VerWeyst & Tucker, 2002). So we also performed the computation assuming that the fluid has no freedom to move in the z-direction. This is achieved by limiting $\hat{C}$ so that its non-zero components are only in the top left two by two submatrix (equivalently considering only the basis elements T_1 and T_2, or only considering the top left two by two submatrix of $\mathcal{M}(\boldsymbol{\kappa}, 0)$), and setting $\theta = 90°$. Computations reveal that $M(\boldsymbol{\kappa}, 0) = 0$. This suggests that to obtain a true sense of how instabilities effect the flow, simulations should allow freedom in all three dimensions, with no symmetry assumptions.

8. Analysis of growth of perturbations

We write the solution of equation (36) as

$$\tilde{B}(t) = L(\boldsymbol{\kappa}_0, t)[\tilde{B}(0)] \tag{76}$$

where $\boldsymbol{\kappa}_0$ is as defined in equation (17), and $L(\boldsymbol{\kappa}_0, t)$ is a linear operator. This can be computed using equations (16), (17), (23), (24), (25), (26), (27), (28), (43), (44), (45), (46), (54) and (50).

By equation (35), we are interested in how much this increases the spectral radius of $\tilde{B}$, which is within a factor of $\sqrt{3}$ from the Frobenius norm of $\tilde{B}$. Thus we are led to solve the equation for the 5×5 matrix $\mathcal{L}(\boldsymbol{\kappa}_0, t)$

$$\frac{\partial}{\partial t}\mathcal{L}(\boldsymbol{\kappa}_0, t) = \mathcal{M}(\boldsymbol{\kappa}, t) \cdot \mathcal{L}(\boldsymbol{\kappa}_0, t) \tag{77}$$

$$\mathcal{L}(\boldsymbol{\kappa}_0, 0) = I \tag{78}$$

and computing the spectral norm of $\mathcal{L}(\boldsymbol{\kappa}_0, t)$. We denote by $n(t)$ the maximum of this spectral norm over all $\boldsymbol{\kappa}_0$ in the two dimensional sphere.

We performed these calculations in the case with shear flow $\boldsymbol{\nabla}\mathbf{u} = \left[\begin{smallmatrix} 0 & 1 & 0 \\ 0 & 0 & 0 \\ 0 & 0 & 0 \end{smallmatrix}\right]$ and $\lambda = 1$ and $\beta = 10$, 100 and 1000. The results are shown in Table 1. Since we are only interested in orders of magnitude, the spectral norms are only calculated to about two digits of accuracy. The calculations were performed with a C++ program, making use of the *Newmat* software package (Davies, 2008) for the matrix calculations, and the *GSL* software package (GNU Scientific Library, 2010) for the elliptic integrals. Also, because the differential equation turned out to be rather stiff, we used the implicit Runge-Kutta method of order 5 (Radau IIA) by Hairer & Wanner (1996*a*,*b*) for solving the ordinary differential equation. The C++ programs may be found at `http://www.math.missouri.edu/~stephen/software/jeff-stokes`.

One can actually follow where the large growths take place, by analyzing the singular decomposition of $\mathcal{L}(\boldsymbol{\kappa}_0, t)$. For example, for the case $t = 10$ and $\beta = 1000$, most of the growth takes place around $\boldsymbol{\kappa}$ in the direction $(\theta, \phi) = (90°, -78.4°)$ (having coming from $\boldsymbol{\kappa}_0$ directed $(\theta, \phi) = (90°, 79°)$), and $\hat{\mathbf{u}}$ is directed parallel to the z-axis. This looks like an extreme form of the 'buckling' effect described above.

A more conservative numerical experiment is to compute the $r(t)$, the maximum over all $\boldsymbol{\kappa}_0$ in the unit sphere of the spectral radius of $\mathcal{L}(\boldsymbol{\kappa}_0, t)$, instead of the spectral norm. We also show the values in Table 1. It may be observed that the

	$\beta = 10$		$\beta = 100$		$\beta = 1000$	
t	$n(t)$	$r(t)$	$n(t)$	$r(t)$	$n(t)$	$r(t)$
1	1.2	1.2	1.3	1.3	1.3	1.3
2	1.3	1.1	1.6	1.2	1.7	1.2
3	2.1	1.3	2.7	1.6	2.7	1.6
4	4	2.1	6	2.8	6.4	2.8
5	6.5	3.7	12	6.4	13	6.9
6	9	5.9	19	13	22	15
7	11	8.1	30	24	38	30
8	12	9.8	48	42	68	59
9	12	11	83	70	140	110
10	11	11	150	120	320	240

TABLE 1. Maximal growth of spectral norm and spectral radius of linearized perturbations starting with isotropic data.

values of the spectral radius are of the same magnitude as the values of the spectral norm.

9. Different Initial Conditions

The actual physical experiments can be performed by pouring the suspension upon a plate, and then running another plate along the top. It is to be expected (and has been reported) that the initial fiber distribution is not isotropic, but rather the effect of the suspension being squeezed by the pouring action is that most of the fibers are aligned in the xz-plane. Squeezing the fluid $\rho > 1$ times can be simulated by a fluid gradient $\boldsymbol{\nabla}\mathbf{u} = \left[\begin{smallmatrix} 1/2 & 0 & 0 \\ 0 & -1 & 0 \\ 0 & 0 & 1/2 \end{smallmatrix}\right]$ running for a time $\log(\rho)$. Thus, this squeezing can be modeled by replacing equation (25) by

$$C = C_\rho \text{ at } t = 0 \tag{79}$$

where

$$C_\rho = \begin{bmatrix} \rho^{-\lambda/2} & 0 & \\ 0 & \rho^{\lambda} & 0 \\ 0 & 0 & \rho^{-\lambda/2} \end{bmatrix} \tag{80}$$

and in the case that U is independent of t, equation (29) is replaced by

$$C = C_\rho \cdot \exp\left(-\tfrac{1}{2}t(\Omega + \lambda\Gamma)\right) \tag{81}$$

Some additional care must be taken in that the solution to equation (33) suggests that equation (34) should be replaced by $\tilde{B} = C_\rho^T \cdot (C^T)^{-1} \cdot \hat{B} \cdot C^{-1} \cdot C_\rho$. However, in view of equation (35), and also that the replacement $\tilde{B}$ fails the requirement $\mathrm{Tr}(\tilde{B}) = 0$, we feel that it is more appropriate to stick with equation (34). However it should be understood that here we are not following the original philosophy. (However for the spectral radius instead of the spectral norm, the two approaches give identical answers.)

In Table 2 we show growth of perturbations for the shear flow $\boldsymbol{\nabla}\mathbf{u} = \left[\begin{smallmatrix} 0 & 1 & 0 \\ 0 & 0 & 0 \\ 0 & 0 & 0 \end{smallmatrix}\right]$ and $\lambda = 1$ and $\beta = 100$ and $\rho = 1$, 2, 3 and 4.

	$\rho = 1$		$\rho = 2$		$\rho = 3$		$\rho = 4$	
t	$n(t)$	$r(t)$	$n(t)$	$r(t)$	$n(t)$	$r(t)$	$n(t)$	$r(t)$
0.5	1.2	1.2	1.7	1.4	3	1.9	4.6	2.6
1	1.3	1.3	2.6	1.8	6.9	3.6	14	6.7
1.5	1.4	1.3	3.9	2.3	14	6.2	39	16
2	1.6	1.2	5.4	2.7	27	10	100	38
2.5	1.9	1.4	7.2	3	49	16	240	84
3	2.7	1.6	9.3	3.2	84	25	570	180
3.5	4	1.8	12	3.2	140	36	1300	360
4	6	2.8	14	3.4	210	51	2700	680
4.5	8.5	4.2	17	4.7	310	67	5400	1300
5	12	6.4	19	6.7	430	81	10000	2200

TABLE 2. Growth of spectral properties with initial data created by squeezing.

Another way the experiment can be performed (see Wang *et al.* (2008)) is to first apply a reverse shear to the suspension until it achieves its steady state, and then to use this as the initial condition. Running a shear in the opposite direction using the Folgar-Tucker equation (Folgar & Tucker, 1984) with $C_I = 0.01$ gives a second order tensor matrix

$$A = \begin{bmatrix} 0.727123 & -0.074765 & 0 \\ -0.074765 & 0.0923099 & 0 \\ 0 & 0 & 0.180567 \end{bmatrix}$$

(this was computed using spherical harmonics (Montgomery-Smith *et al.*, 2010*b*,*c*)), which by inverting the elliptic integrals (see Montgomery-Smith *et al.*, 2010*a*), can be shown to correspond to

$$C = \begin{bmatrix} 0.372914 & 0.216212 & 0 \\ 0.216212 & 2.20872 & 0 \\ 0 & 0 & 1.28714 \end{bmatrix}$$

(Note that C is uniquely determined from B up to pre-multiplication by an orthogonal matrix, and pre-multiplying C by an orthogonal matrix has the effect of changing $\tilde{B}$ by an orthogonal change of basis, which does not change its spectral norm.) Using this value of C as the initial data, and applying the above shear with $\lambda = 1$ and $\beta = 100$ gave the results shown in Table 3.

It can be seen that both sets of initial conditions illustrated here give rise to growths of perturbations that greatly exceed the growth with isotropic initial conditions.

10. Floquet Theory

Here we produce results according to the Floquet method. This is a well established theory for ordinary differential equations (see, for example, Chicone, 2006), and provides sufficient conditions for periodic solutions to differential equations to be stable or unstable. Because we are working with a partial differential equation, the results from this section should not be regarded as mathematically rigorous, but we hope to produce rigorous versions of these results in future works.

t	$n(t)$	$r(t)$
0.5	4.7	2.9
1	14	6.8
1.5	37	13
2	81	22
2.5	160	29
3	280	43
3.5	470	130
4	720	290
4.5	1100	540
5	1500	900

TABLE 3. Growth of spectral properties with initial data created by a reverse shear.

Consider the shear flow $\boldsymbol{\nabla}\mathbf{u} = \left[\begin{smallmatrix} 0 & 1 & 0 \\ 0 & 0 & 0 \\ 0 & 0 & 0 \end{smallmatrix}\right]$ with $|\lambda| < 1$. Then the solution to the unperturbed equation is periodic with period $T_p = 2\pi/\sqrt{1-\lambda^2}$. For any multiple $n \geq 1$ of T_p, we have

$$\mathcal{L}(\boldsymbol{\kappa}_0, nT_p) = \mathcal{L}(e^{-(n-1)T_p U^T}\boldsymbol{\kappa}_0, T_p) \cdot \mathcal{L}(e^{-(n-2)T_p U^T}\boldsymbol{\kappa}_0, T_p) \cdots \mathcal{L}(\boldsymbol{\kappa}_0, T_p) \tag{82}$$

and furthermore $e^{-tU^T}\boldsymbol{\kappa}_0$ converges to a direction parallel to the y-axis as $t \to \infty$. Since $\mathcal{L}(\boldsymbol{\kappa}, T_p)$ is continuous in $\boldsymbol{\kappa}$, it follows that stability of $\mathcal{L}(\boldsymbol{\kappa}_0, nT_p)$ as $n \to \infty$ is the same as stability of $\mathcal{L}(\mathbf{e}_2, T_p)^n$, where $\mathbf{e}_2$ is the unit vector parallel to the y-axis. Thus if we can show that any of the eigenvalues of $\mathcal{L}(\mathbf{e}_2, T_p)$ have absolute value greater than one, then the perturbations of B are linearly unstable.

For example, if $\lambda = 0.8$ (when $T_p \approx 10.472$) and $\beta = 100$, then the largest absolute value of the eigenvalues is about $89,000$. This indicates great instability. We propose that this instability breaks up the periodic behavior, and causes the loss of orientation memory described in Anczurowski & Mason (1967).

11. Conclusion

The results from Tables 1, 2 and 3 show that the size of $\tilde{B}$ increases by a fairly substantial amount. If the original perturbations are reasonably large, one can see that even after a short amount of time, that large deviations from the unperturbed solution are very likely. We propose that this is what leads to the greatly reduced rate of alignment of the fibers.

We suspect that the perturbations will take place at small length scales, in both numerical and physical experiments. The reason we think this is as follows. The rate of growth of the perturbations does not depend upon the size of the wave number. One of our assumptions is that the medium is of infinite extent. If we have the more realistic situation where there are boundaries to the medium, it is reasonable to think that if the wave number is smaller (that is, the length scale of the oscillations of the perturbations is larger), that the boundary has a greater effect, and that most likely this effect slows down the growth. Thus we think that the perturbations take place with large wave numbers. The largest realistic wave number for physical experiments is probably the reciprocal of the length of the fibers, and in numerical experiments is probably the reciprocal of the size of

the spacial grid or elements used. For this reason, we suspect that the growth of perturbations may be quite difficult to measure in physical experiments, and in numerical experiments might be mistaken for problems with the numerical method. Indeed, when one is operating at these kinds of small length scales, one begins to doubt even the assumption that discrete fibers can be well represented by the continuum.

For future work, we would like to see the result of a full numerical simulation of the coupled Jeffery-Stokes equation, that is, equations (3), (5), (6), (21) and (26), replacing equation (22) with B initially set to a small perturbation of I. We note that some numerical simulations of the coupled equations have already been performed Chinesta & Poitou (2002); Chinesta *et al.* (2003); VerWeyst & Tucker (2002), but we believe that more detailed computations, that allow complete freedom in all three spacial dimensions, are necessary to observe the effects predicted in this paper.

12. Acknowledgments

The author gratefully acknowledges support from N.S.F. grant C.M.M.I. 0727399.

References

Anczurowski, E. & Mason, S.G. 1967 The kinetics of flowing dispertions iii. equilibrium orientation of rods and discs (experimental). *J. Colloid Int. Sci.* pp. 533–546.

Bird, R.B., Curtiss, C.F., Armstrong, R. C. & Hassager, O. 1987 *Dynamics of Polymeric Liquids*, 2nd edn., , vol. 2: Kinetic Theory. New York, NY: John Wiley & Sons, Inc.

Carlson, B.C. 1995 Numerical computation of real or complex elliptic integrals. *Journal Numerical Algorithms* **10**, 13–26.

Chicone, C. 2006 *Ordinary Differential Equations with Applications*, 2nd edn. New York: Springer-Verlag.

Chinesta, F., Chaidron, G. & Poitou, A. 2003 On the solution of Fokker-Planck equations in steady recirculating flows involving short fiber suspensions. *Jn. of Non-Newtonian Fluid Mechanics* **113**, 97–125.

Chinesta, F. & Poitou, A. 2002 Numerical Analysis of the Coupling Between the Flow Kinematics and the Fiber Orientation in Eulerian Simulations of Dilute Short Fiber Suspensions Flows. *The Canadian Journal of Chemical Engineering* **80**, 1107–1114.

Davies, R. 2008 Newmat C++ matrix library, `http://www.robertnz.net/nm_intro.htm`.

Dinh, S.M. & Armstrong, R.C. 1984 A Rheological Equation of State for Semiconcentrated Fiber Suspensions. *Jn. of Rheology* **28** (3), 207–227.

Folgar, F.P. & Tucker, C.L. 1984 Orientation Behavior of Fibers in Concentrated Suspensions. *Jn. of Reinforced Plastics and Composites* **3**, 98–119.

GNU Scientific Library 2010 GNU Scientific Library, `http://www.gnu.org/software/gsl`.

Hairer, E. & Wanner, G. 1996*a* `http://www.unige.ch/~hairer/prog/stiff/radau5.f`.

Hairer, E. & Wanner, G. 1996*b* *Solving Ordinary Differential Equations. Stiff and Differential-Algebraic Problems*. New York: Springer-Verlag.

Jeffery, G.B. 1923 The Motion of Ellipsoidal Particles Immersed in a Viscous Fluid. *Proceedings of the Royal Society of London A* **102**, 161–179.

Lipscomb II, G.G., Denn, M.M., Hur, D.U. & Boger, D.V. 1988 Flow of Fiber Suspensions in Complex Geometries. *Jn. of Non-Newtonian Fluid Mechanics* **26**, 297–325.

Montgomery-Smith, S.J., He, W., Jack, D.A. & Smith, D.E. 2010*a* Exact tensor closures for the three dimensional Jeffery's Equation. *preprint available at* `http://www.math.missouri.edu/~stephen/preprints/exact-closure.html` .

Montgomery-Smith, S.J., Jack, D.A. & Smith, D.E. 2010*b* Spherical software package, `http://www.math.missouri.edu/~stephen/software/spherical`.

Montgomery-Smith, S.J., Jack, D.A. & Smith, D.E. 2010*c* A Systematic Approach to Obtaining Numerical Solutions of Jeffery's Type Equations using Spherical Harmonics. *Composites Part A* **41**, 827–835.

Nguyen, N., Bapanapalli, S.K., Holbery, J.D., Smith, M.T., Kunc, V., Frame, B., Phelps, J.H. & Tucker, C.L. 2008 Fiber Length and orientation in Long-Fiber Injection-Molded Thermoplastics - Part I: Modeling of Microstructure and Elastic Properties. *Jn. of Composite Materials* **42** (10), 1003–1029.

Sepehr, M., Carreau, P.J., Grmela, M., Ausias, G. & Lafleur, P.G. 2004 Comparison of Rheological Properties of Fiber Suspensions with Model Predictions. *Jn. of Polymer Engineering* **24** (6), 579–610.

Strogatz, S.H. 1994 *Nonlinear Dynamics and Chaos*. Perseus Books.

Szeri, A.J. & Lin, D.J. 1996 A deformation tensor model of brownian suspensions of orientable particles —the nonlinear dynamics of closure models. *Journal of Non-Newtonian Fluid Mechanics* **64**, 43–69.

Verleye, V. & Dupret, F. 1993 Prediction of Fiber Orientation in Complex Injection Molded Parts. In *Developments in Non-Newtonian Flows*, pp. 139–163.

VerWeyst, B.E. 1998 Numerical Predictions of Flow Induced Fiber Orientation in Three-Dimensional Geometries. PhD thesis, University of Illinois at Urbana Champaign.

VerWeyst, B.E. & Tucker, C.L. III 2002 Fiber Suspensions in Complex Geometries: Flow-Orientation Coupling. *The Canadian Journal of Chemical Engineering* **80**, 1093–1106.

Wang, J., O'Gara, J.F. & Tucker, C.L. 2008 An objective model for slow orientation kinetics in concentrated fiber suspensions: Theory and rheological evidence. *J. Rheology* **52**, 1179–1200.

Department of Mathematics, University of Missouri, Columbia MO 65211, U.S.A.